ACS Chemical Neuroscience

Research Article

pubs.acs.org/chemneuro

Influence of the Physiochemical Properties of Superparamagnetic Iron Oxide Nanoparticles on Amyloid β Protein Fibrillation in Solution

Morteza Mahmoudi,*[,†,‡] Fiona Quinlan-Pluck,[§] Marco P. Monopoli,[§] Sara Sheibani,[∥] Hojatollah Vali,[⊥] Kenneth A. Dawson,[§] and Iseult Lynch*[,§]

[†]Department of Nanotechnology and [‡]Nanotechnology Research Centre, Faculty of Pharmacy, Tehran University of Medical Sciences, Tehran, Iran

[§]Centre for BioNano Interactions, School of Chemistry and Chemical Biology, & Conway Institute of Biomolecular and Biomedical Sciences University College Dublin, Belfield, Dublin 4, Ireland

[∥]Department of Chemistry and Chemical Engineering, Royal Military College, Kingston, Ontario K7K 7B4, Canada

[⊥]Department of Anatomy and Cell Biology, McGill University, Montreal, Canada

Supporting Information

ABSTRACT: Superparamagnetic iron oxide nanoparticles (SPIONs) are recognized as promising nanodiagnostic materials due to their biocompatibility, unique magnetic properties, and their application as multimodal contrast agents. As coated SPIONs have potential use in the diagnosis and treatment of various brain diseases such as Alzheimer's, a comprehensive understanding of their interactions with Aβ and other amyloidogenic proteins is essential prior to their clinical application. Here we demonstrate the effect of thickness and surface charge of the coating layer of SPIONs on the kinetics of fibrillation of Aβ in aqueous solution. A size and surface area dependent "dual" effect on Aβ fibrillation was observed. While lower concentrations of SPIONs inhibited fibrillation, higher concentrations increased the rate of Aβ fibrillation. With respect to coating charge, it is evident that the positively charged SPIONs are capable of promoting fibrillation at significantly lower particle concentrations compared with negatively charged or uncharged SPIONs. This suggests that in addition to the presence of particles, which affect the concentration of monomeric protein in solution (and thereby the nucleation time), there are also effects of binding on the protein conformation.

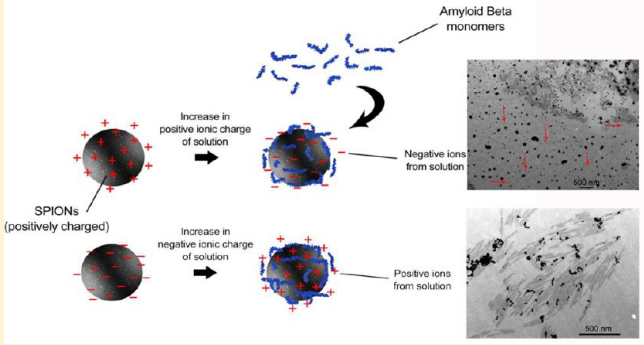

KEYWORDS: *Superparamagnetic iron oxide nanoparticles, Alzheimer's disease, amyloid beta, fibrillation, protein conformation*

Alzheimer's disease is a well-known progressive neurodegenerative brain disorder linked to aggregation of amyloid-β (Aβ) and tau proteins, resulting in the formation of insoluble extracellular plaques. The mode of aggregation and the mechanism of interaction of these plaques with cellular components in the brain are poorly understood. Understanding the molecular machinery resulting in Alzheimer's disease is crucial to the development of new drugs and to finding therapeutic solutions. There is debate concerning the mechanism(s) involved in fibrillation and the toxic effect of fibrils on nerve cells, and it has been suggested that small, oligomeric protein clusters are involved in cell damage.[1,2] Aβ is an amphipathic polypeptide with molecular weight of 4 kDa, consisting of 36−43 amino acids; the self-assembly of Aβ resulting in fibril formation is believed to have a crucial role in the onset and progression of Alzheimer's disease. Similar protein fibrillation processes have been implicated in other amyloidogenic diseases, such as Parkinson's disease.[3−5] The deposition of insoluble protein fibrils in the brain is a crucial event in Alzheimer's pathology.[6,7] The characteristic feature of the fibrillar form of Aβ is the existence of a cross-β structure with stacking of β strands perpendicular to the long axis of the fiber.[8] The monomeric Aβ is relatively unstructured in solution.[9]

The first 16 residues of Aβ are highly charged, however, the rest of the sequence contains two stretches of hydrophobic residues (16−20) and (30−40), which are believed to play a crucial role in oligomerization, separated by a region containing two acidic (Glu 22 and Asp 23) and one basic (Lys 28) residues.[10] It has been suggested that the hydrophobic core plays a key role in the aggregation of Aβ; hence, modifications

Received: November 1, 2012
Accepted: December 26, 2012
Published: December 26, 2012

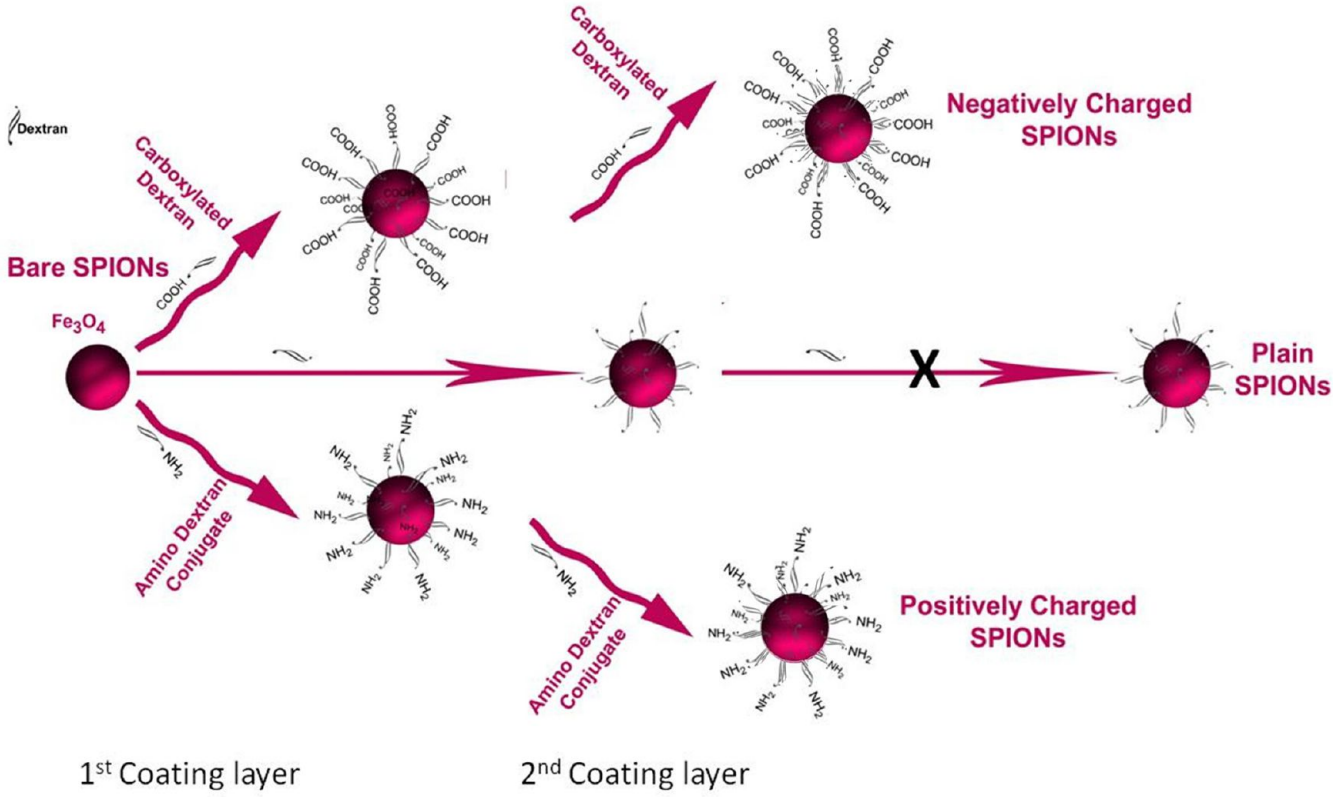

Figure 1. Scheme showing the how the various single- and double-coated SPIONs were prepared. Note that, in the case of the plain particles, the second coating layer was not very successful.

of the hydrophobic part can accelerate or inhibit fibril formation and promote/induce the disassembly of Aβ fibrils.[11−14]

It appears that abnormal folding of the monomeric Aβ results in the formation of an oligomeric state and subsequently deposition of insoluble (fibrillar) states.[15] According to previous reports, specific charge−charge interactions of the amyloidic-polypeptide structure play a key role in the formation of the oligomeric states.[16−18] However, these reports are controversial[19] and further investigation is needed to clarify the details of the oligomerization and fibrillation processes.[20]

It is well-known that the aggregation kinetics of amyloidogenic proteins and peptides follow a sigmoidal kinetics, whereby the process starts with a lag phase (i.e., the activation time required for a "critical" nucleus to form) followed by rapid elongation proceeding to the formation of mature fibrils.

Small biological molecules such as peptides and nonpeptides (e.g., inositols, phenols, and indols) have been shown to interfere with the formation of fibrils by influencing the kinetics of aggregation.[21−25] Many amyloidogenic proteins have a tendency to be absorbed at the surface of a variety of substrates; hence, nanoparticles, with their small size and large surface to volume ratio, have a significant effect on the fibrillation process of a wide range of amyloidogenic proteins.[26−28] More specifically, some nanoparticles, such as copolymers of NIPAM:BAM (*N*-siopropylacrylamide:*N*-*tert*-butylacrylamide), can delay the fibrillation process through interactions with either the monomeric peptide or oligomeric compounds, resulting in a decrease of the concentration of the monomers/oligomers in solution, and leading to a significant increase in the lag time and thus inhibition of polymerization.[29] Cabaleiro-Lago et al.[30] have shown that the ratio of surface area of the substrate to peptide concentration determines the effect of cationic polystyrene nanoparticles on Aβ fibrillation. Depending on the specific ratio (i.e., between the peptide and particle concentration), the kinetic effects of amine-modified polystyrene nanoparticles varied from acceleration of the fibrillation process by reducing the lag phase (at low particle surface area in solution) to inhibition of the fibrillation process at high particle surface area, suggesting a dual effect on the rate of Aβ fibrillation.

Among the various nanoparticles used in biomedical research, functionalized superparamagnetic iron oxide nanoparticles (SPIONs) have been recognized as promising materials due to their high biocompatibility, unique magnetic properties, and their capacity for use as multimodal contrast agents.[31−34] However, the use of SPIONs in the clinics in the context of diagnosis of brain diseases is still extremely limited.[35−38] There is potential for nanoparticles with high affinity for the circulating Aβ forms to induce a "sink effect"[39] and, thus, potentially ameliorate Alzheimer's disease. Therefore, since SPIONs are proposed for use as theranostic agents (i.e., simultaneous diagnosis and treatment) in various brain diseases,[40−42] understanding their interactions with Aβ and other amyloidogenic proteins is essential to ensure that their medical use does not inadvertently contribute to amyloid related disease progression.

There are only a few reports on the interaction of SPIONs with amyloidogenic proteins in the literature,[43−47] and the majority of them are focused on insulin amyloid fibril formation. As SPIONs are recognized as the most prominent candidate (although studies are still in their infancy) for multitask simultaneous biomedical applications,[48−50] the main focus of this study is to assess the effect of the physiochemical

dx.doi.org/10.1021/cn300196n | *ACS Chem. Neurosci.* 2013, 4, 475−485

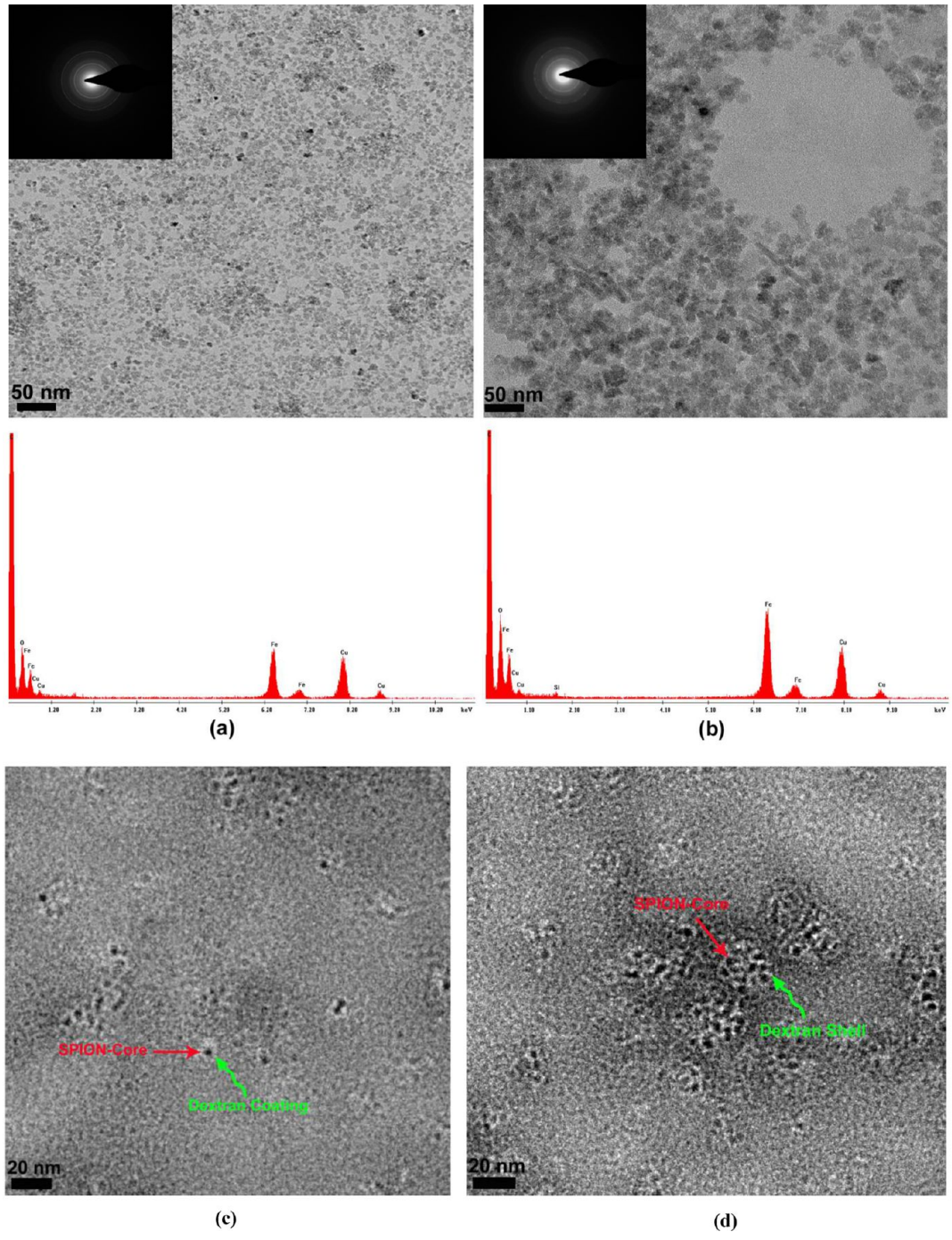

Figure 2. (a,b) TEM images (scale bar = 50 nm) of single- and double-coated SPIONs with the COOH-dextran coating (upper left panels are selected area diffraction pattern) and their corresponding energy dispersive X-ray spectroscopy results. (c, d) TEM images of single- and double-coated SPIONs with the COOH-dextran coating with higher magnification; there is clear evidence of aggregation of SPIONs in (d) explaining the larger size, as also measured in DLS.

properties of SPIONs and their polymeric coating composition on the kinetic of Aβ fibrillation.

RESULTS AND DISCUSSION

Transmission electron microscopy (TEM) analysis of the single-coated (small, S-) and double coated (large, L-) negative SPIONs revealed similar morphological characteristics to the SPIONs with plain and positive surface charges (see Figures 1 and 2). The results showed that the SPIONs were synthesized with a narrow size distribution (Supporting Information Figures S1 and S2). High-resolution lattice fringe images and the electron diffraction pattern of the particles are consistent with the structure of nanocrystalline magnetite (Figure S3).

The SPION sizes, size distributions, and surface charge were also determined, and the results of dynamic light scattering (DLS) and zeta potential experiments are summarized in Table 1 for all samples. According to the data displayed in Table 1, the average TEM diameter of single-coated particles is ~15 nm (with the iron oxide core being ~5 nm); however, the DLS results are highly dependent on the surface chemistry of the

dx.doi.org/10.1021/cn300196n | ACS Chem. Neurosci. 2013, 4, 475−485

Table 1. Description of the Various SPIONs in DI Water

sample/size (nm)	functional group	TEM Size (nm)	D_H (nm)[a]	PDI[b]	$\langle D_H \rangle$ (nm)[c]	ζ potential (mV)[d]	nickname
no coating[e]	OH	5 ± 0.5					bare
single dextran coated	COOH		39.7 ± 0.1	0.169	48.6 ± 0.6	−21.4 ± 0.4	S-negative
	plain	15.2 ± 1.2	74.0 ± 1.0	0.209	87.6 ± 4.5	−9.1 ± 0.7	S-plain
	NH_2		105.1 ± 6.2	0.248	92.0 ± 2.5	+19.3 ± 0.5	S-positive
double dextran coated	COOH		64.6 ± 1.3	0.24	74.2 ± 4.0	−17.8 ± 0.3	L-negative
	plain	[f]	78.6 ± 0.81	0.223	93.8 ± 5.4	−6.2 ± 0.9	L-plain
	NH_2		179.5 ± 3.02	0.24	225.7 ± 11.2	+9.3 ± 1.1	L-positive

[a] *z*-Average hydrodynamic diameter extracted by cumulant analysis of the data from DLS measurements (see Figure S1). [b] Polydispersity index. [c] Average hydrodynamic diameter determined from CONTIN size distribution (see Figure S2). [d] Zeta potential measurements were determined in low ionic strength solutions to ensure electrophoretic mobility. [e] Confirmed by TEM images (see Figure 2). [f] Difficult to determine since the dextran layer is weakly scattering and there may be some agglomeration of particles during drying.

SPIONs' dextran coating (see Figures S1 and S2). More specifically, the hydrodynamic size of the negatively charged dextran coated SPIONs is significantly smaller than that of the positively charged dextran coated ones, suggesting different degrees of swelling/hydration of the dextran layers. The addition of the second layer of dextran increased the DLS hydrodynamic diameters for the negatively and positively charged SPIONs. In the case of the plain SPIONs, it appears that a second dextran layer did not form as no change in particle size was observed by DLS. This suggests that the immobilized number of ions and the water layer at the surface of the SPIONs are highly dependent on the surface charge and size of the SPIONs, and that this should be considered in the description of protein absorption and fibrillation phenomena.

The effect of SPIONs with different size, charge and surface treatment on Aβ aggregation in solution at different SPION concentrations was investigated. The optimal concentration of Aβ (0.5 μM) was determined by ThT fluorescence probing of the aggregation kinetics at various Aβ concentrations (see Figure S4). The main reason for the choice of the low concentration of Aβ was to analyze the effects of different SPIONs on the amyloid fibrillation process in an experimentally feasible time frame. At this concentration, shifts in the nucleation lag time in either direction are recognizable relative to the kinetics of Aβ alone. Note that the fibrillation of Aβ at the selected concentration illustrated all three stages of a typical protein fibrillation, that is, lag phase, elongation phase, and steady state. The fibrillation of 0.5 μM synthetic Aβ in vitro was clearly affected by the SPION concentration (40−100 μg/mL) and the physiochemical properties of the SPIONs dextran coating (Figure 3). The presence of SPIONs essentially affected either the lag phase or the elongation rate of the Aβ fibrillation. Previously examined nanoparticles (e.g., polymeric, TiO_2, and dendrimers) showed significant changes in the lag time, while the elongation stage was not changed significantly compared to the control.[27,28]

Figure 3 reveals interesting phenomena associated with the Aβ fibrillation process in the presence of SPIONs. The most striking finding was the dual effect of positively charged double-coated SPIONs on the kinetics of Aβ fibrillation. These particles were shown to have a concentration dependent effect on Aβ fibrillation; at lower particle concentrations, they inhibited fibrillation or had no effect on fibrillation (40 and 60 μg/mL). At higher concentrations (80 and 100 μg/mL), they promoted fibrillation by decreasing the nucleation lag time. Similar charge effects (at low nanoparticles/Aβ concentration) have been observed with amine-modified polystyrene nanoparticles and amine-modified artificial chaperones with respect to the ratio of available particle surface area to Aβ concentration.[30,51] At lower concentration of Aβ, due to their negative net charge, the Aβ monomers would attach to the surface of the positively charged SPIONs, resulting in an inhibitory effect of positive SPIONs on fibrillation. However, it has been shown that the inhibitory effect of amine-modified particles is strongly dependent on the surface composition of the particles.[52]

In addition, the single layer positively charged SPIONs showed no accelerating effect on Aβ fibrillation at any of the examined concentrations while the lag time was reduced significantly with increasing concentration of these particles (the same trend was observed with the double-layer positively charged SPIONs at concentrations below 60 μg/mL). It is also worth noting that the zeta potential of the single layer positive SPIONs was significantly more positive than that of the double layer positive SPIONs (+19 versus +9, respectively). This explained the difference in the observed results as the density of positive charge at the SPION surface coupled to SPION surface curvature could influence the absorbed protein conformation. Thus, it seems that there is competition between Aβ binding to the surface of SPIONs, which could increase the lag time (by decreasing the solution concentration such that the critical nuclei cannot form), and the effect of the positive charge on the conformation of the adsorbed Aβ. Thus, the positive charge at the surface of SPIONs can induce conformational changes to the amyloid monomers, which could result in a significant decrease in the lag time if the altered protein conformation is more prone to fibrillation (see Figure S6). One possible explanation for this observation could be the physical (i.e., electrostatic) interactions of positively charged SPIONs with negatively charged segments of the Aβ backbone (such as with the carboxylate groups on the Aβ proteins in Asp and Glu residues). Previous reports confirmed the importance of the charge−charge interactions between imidizolium groups on His residues and carboxylate groups on Asp and Glu residues[16,18,53] for Aβ fibrillation.

In contrast to the positive SPIONs, the negative SPIONs (both S-negative and L-negative) are shown to delay or inhibit the fibrillation process in a concentration and size dependent manner. The fibrillation process was inhibited completely with both the single and double layer COOH-dextran coated SPIONs even at very low (i.e., 40 μg/mL) particle concentrations. This became less effective as the SPION

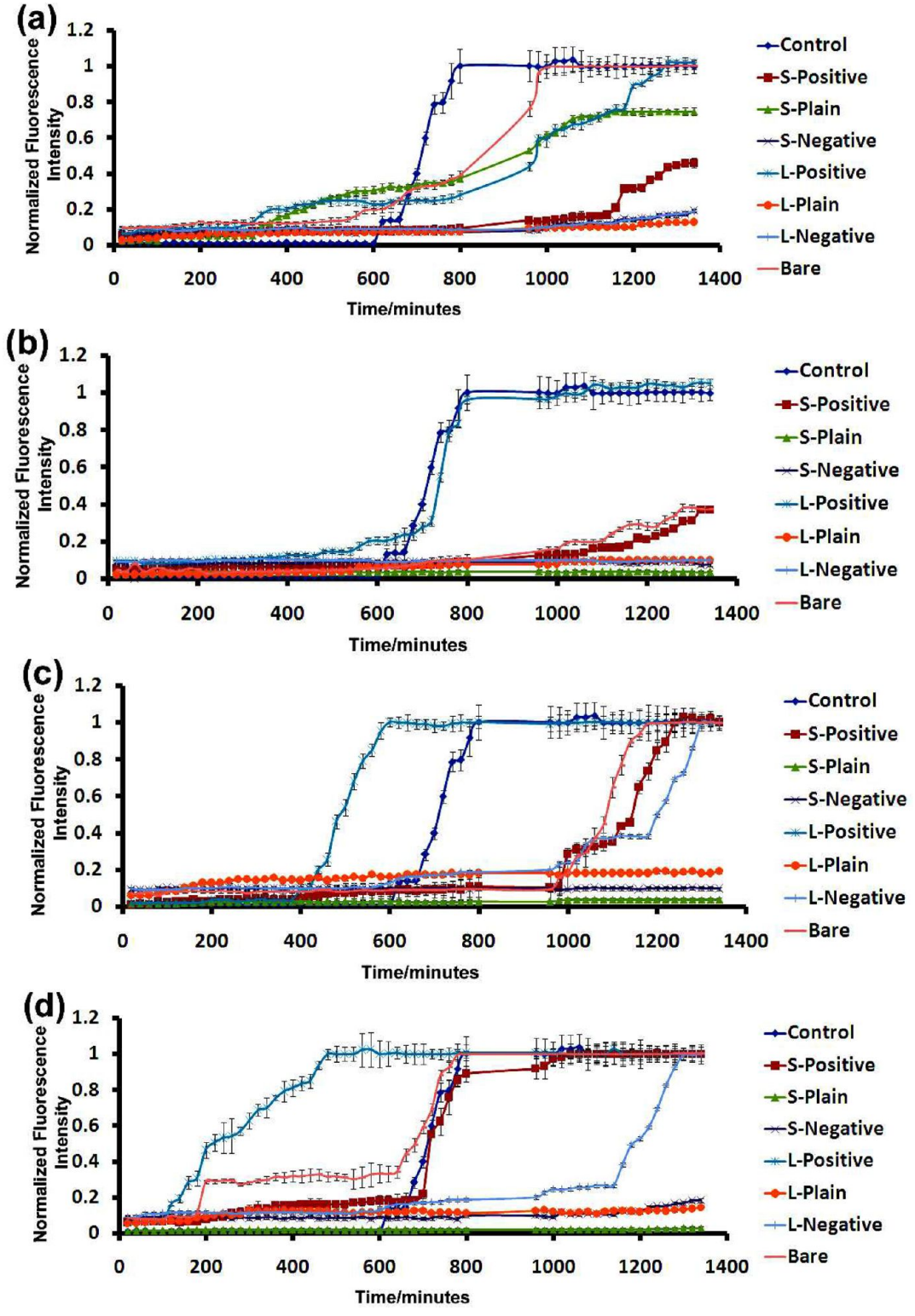

Figure 3. Kinetics of aggregation of Aβ in the absence or presence of various single and double (negative, positive, and plain) dextran-coated SPIONs at different SPION concentrations including (a) 40 μg/mL, (b) 60 μg/mL, (c) 80 μg/mL, and (d) 100 μg/mL.

concentration increased (although these particles were still inhibitory in nature, as the lag time remained longer than that of Aβ alone). In this case, the surface charge of both single and double layer negative SPIONs was similar, at −21.4 and −17.8, respectively. It was obvious that SPION surface area was an important factor: decreasing the SPION size from 64.6 nm (double-coated) to 39.7 nm (single-coated) (Table 1) led to a significant increase in the lag time (Figure 3).

The plain SPIONs showed the same trend as the negative particles. By increasing the concentration of the particles the lag time was increased, and for most of the particles, there was no trace of an elongation stage during the examined time (i.e., 1340 min). The hydrodynamic sizes of the single- and double-

dx.doi.org/10.1021/cn300196n | ACS Chem. Neurosci. 2013, 4, 475−485

coated plain SPIONs were identical, and their zeta potentials were also very similar, with both being slightly negatively charged (−9.1 and −6.2, respectively, see Table 1).

Since the central hydrophobic region of Aβ (16−20) is responsible for Aβ (1−42) self-recognition and assembly (i.e., creation of mature fibrils with a diameter of 7−10 nm),[54] a possible mechanism for the strong retardation effect of negative SPIONs may be related to interaction of the SPION surface charge with the hydrophobic core of the Aβ peptide. We suggested that the negative particles, more specifically the carboxylated SPIONs, can interact with the amide backbone of the Aβ (16−20) core. If so, it is expected that the hydrophobic core would be considerably modified leading to a strong inhibition of the fibril formation. This explanation is consistent with previous reports showing that modification of the amide backbone with N-methyl amino acids,[55,56] ester linkages,[57] and isostructural E-olefin bonds[58]could not only disrupt fibril formation but could also induce the disassembly of already formed fibrils. The observation of enhanced fibrillation at higher concentrations of the double layer negative SPIONs suggests that a stronger interaction between Aβ and the dextran backbone occurs at higher particle concentrations. This results in a fibrillation-competent conformation of Aβ at the higher particle concentrations, and thus fibrillation was accelerated.

In addition to charge, size is also an important factor in the effect of both positive and negative dextran-coated SPIONs on Aβ fibrillation. By decreasing the SPION size (via the coating thickness), the inhibitory effect of the particles was increased, which is consistent with a previous report showing the importance of the amount of available surface area for peptide adsorption on the inhibition effects of polymeric nanoparticles.[59]

Finally, bare SPIONs showed dramatic effects on Aβ fibrillation, showing stop-start type behavior, whereby there appear to be multiple short bursts of fibrillation followed by plateaus, followed by another burst of fibrillation.[19] However, due to the highly agglomerated state of the plain SPIONs, it was difficult to obtain any trends regarding their effect on the elongation phase of Aβ fibrillation.

In addition to the known mechanisms, the local pH effects of the various SPIONs could potentially contribute to the obtained results. Upon addition of the positive SPIONs to a solution containing Aβ, the surfaces of the particles would be covered by the anions present in the medium. In this case, the concentration of the positive charges (which bind to the free Aβ monomers) would be decreased. Previous reports have shown the importance of the pH on Aβ fibrillation.[3,10] The effect of pH (2 and 12) on Aβ fibrillation was studied at a concentration of 0.5 μM, (Figure S5). According to these results, the isoelectric point of Aβ was located at approximately pH 5.5, which was in good agreement with other reports.[3,10] In addition, after adding 100 μL of single-coated negative- and positive-SPIONs, the pH changed in the amyloid solution. The particles were removed from the amyloid media using an external magnetic field; in this case, the pH of the remaining solutions (i.e., free from particles) was 6.8 ± 0.3 and 7.9 ± 0.4 after interaction with negative- and positive-SPIONs, respectively. It is notable that the initial pH was fixed at 7.4. We observed that the Aβ fibrillation rate was not greatly affected by pH in the range of pH 6.8−7.9 (Figure S5). Therefore, an effect from SPIONs altering the solution pH on Aβ fibrillation rate can be ruled out.

The effect of the surface charges associated with the various dextran coated SPIONs on Aβ fibrillation are summarized in Figure S6. By increasing the concentration of the double-coated SPIONs, a clear decrease in lag time can be observed. On the other hand, the double-coated negatively charged and plain SPIONs show a clear inhibition of fibrillation (Figure S6). Similar data were obtained with the single-layer dextran coated series of SPIONs, suggesting a reduction in the lag time at the highest SPION concentration, for the positive SPIONs.

TEM images of the control sample (Aβ in the absence of SPIONs, at 0.5 μg/mL) obtained after 700, 1200, and 2400 min incubation are shown in Figure 4. The fibrils are short and have a very broad size distribution in the early fibrilation stage (Figure 4a); however, the size of the fibrils increased and their size distribution narrowed significantly with increasing incubation time. The blue arrows in Figure 4a show small fibrils that are attached to larger aggregates. It is interesting to note that although the ThT results shows that the fibrillation process was finished after 800 min of incubation (Figure 3), TEM images revealed that polymerization of the fibrils leading to the formation of larger aggregate continues during incubation for longer times. It is possible that as the total number of intercolation sites is the same, ThT is not able to measure the complete polymerization reaction.

Addition of the negative and plain dextran coated SPIONs (both single and double layer) resulted in a decrease of the fibril size and a narrower size distribution (see Figure 5) compared to the Aβ fibrils formed in the absence of SPIONs. In both cases, an increase of the fibrillation lag time was also observed in the ThT assay, together with lower fibrillation rates. Thus, it appeared that negatively charged SPIONs (Table 1) delayed the Aβ fibrillation process, resulting in more homogeneous growth of fibrils during the oligomerization phase. In contrast, positively charged SPIONs caused the formation of fibrils with a very broad size distribution (Figure 5). The fibril sizes are estimated from the TEM images in the absence and presence of SPIONs with different surface charge are shown in Figure S7. More details of the fibrillation process and driving force for this process are given in the Supporting Information section.

In order to assess the effect of the SPION dextran coating charge and thickness on any secondary structural changes of Aβ, far-UV circular dichroism (CD) spectroscopy was employed. Representative results are shown in Figure 6 with the data for all particles shown in Table S1. The CD spectra of monomeric (random coil structure) Aβ monomers had a characteristic, intense minimum and a maximum at 200 and 220 nm, respectively (Figure 6), which is consistent with a random coil conformation. After completion of the fibrillation process (based on the ThT fluorescence results) where Aβ monomers are converted to fibrils (i.e., 1340 min at 37 °C), the CD spectrum revealed changes in the wavelength and intensities of the maxima and minima, due to changes in the Aβ secondary conformation. This indicated the formation of a β-sheet conformation (β-sheet-rich assemblies; minimum wavelength at 214 nm) (Figure 6). The CD spectra results of Aβ fibrillation in the presence of positive-dextran-coated SPIONs confirmed the ThT fluorescence results. This also showed the formation of severe β-sheet assemblies regardless of the thickness of the SPION particles' dextran coating. In contrast, Aβ in the presence of negative- and plain-dextran-coated SPIONs continued to illustrate the characteristics of the random coil, suggesting no induction of conformational change

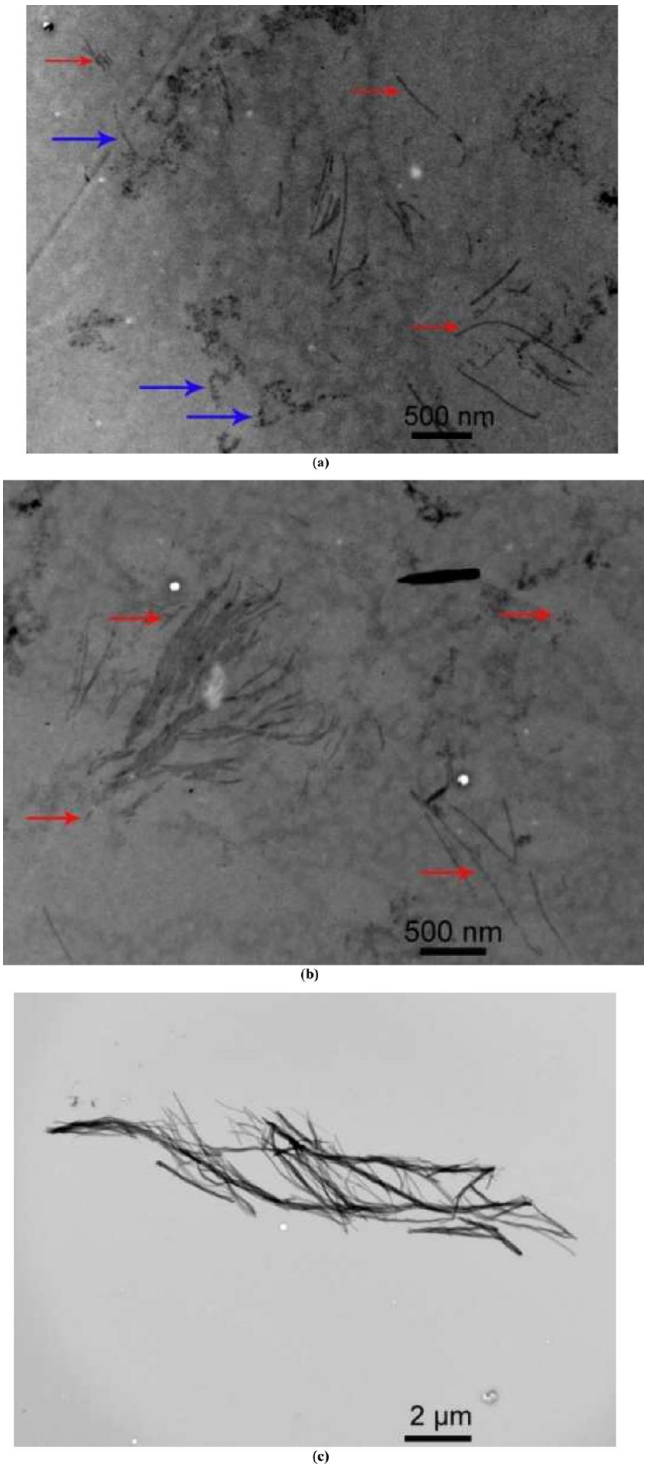

Figure 4. TEM images of Aβ fibrils after incubation for (a) 700 min, (b) 1200 min, and (c) 2400 min in the absence of SPIONs. Protein concentration is 0.5 μM.

as a result of the presence of these SPIONs. The results obtained were fully consistent with the previous reports on the CD study of various employed molecules/particles for retardation and acceleration of lag time in Aβ fibrillation.[60]

CONCLUSIONS

The present study on the effect of SPION nanoparticles on Aβ fibrillation investigated several physicochemical parameters, such as the charge on the dextran polymer coating and the thickness of the dextran coating (i.e., a single polymer layer or a double polymer layer) on the lag time before onset of Aβ fibrillation. It was shown that particle size has significant effects on the Aβ fibrillation process; thus, a practical problem that may be encountered is the size distribution of nanoparticles in the commercially available SPIONs. We have previously shown that nanoparticles can affect protein fibrillation in two distinct ways: either enhancing the rate of fibrillation (increasing the likelihood and occurrence of nucleation) or inhibiting the rate of fibrillation (reducing the likelihood and occurrence of nucleation).[30] In both cases, the observed effects can be a result of changes in local protein concentration and/or changes in protein conformation. Indeed, dual effects have also been observed, whereby the effects observed were dependent on the ratio of particle surface area to protein concentration, showing the subtle interplay of local concentration and protein conformation on formation of the critical nuclei. These are stochastic events and are the first step in the fibrillation processes.

Depending on the surface coating charge, a surface area dependent "dual" effect was observed, with lower concentrations of SPIONs inhibiting fibrillation, while higher concentrations enhanced the rate of Aβ fibrillation. Coating charge influenced the concentration at which the acceleratory effects were observed, with the positively charged SPIONs promoting fibrillation at significantly lower particle concentrations than either negatively charged or essentially uncharged (plain) SPIONs. This suggested that in addition to the presence of SPIONs affecting the concentration of monomeric protein in solution (and thereby the nucleation time), there were also effects of binding on the Aβ conformation, which was mainly detected with the positively charged SPIONs.

The data suggested that SPIONs designed for medical imaging applications in vivo should consider using a negatively charged or uncharged surface coating preferentially, as these are less likely to induce undesired side effects such as protein fibrillation, while maintaining the desired magnetic function. Interestingly, this has also been shown in the in vivo simulated situations (i.e., where the effect of protein pre-coated nanoparticles on Aβ fibrillation was investigated).[61] Furthermore, the observed results regarding the kinetics of fibrillation should be further examined in vivo. Very recently, SPIONs administered intravenously to APP transgenic mouse models of Alzheimer's disease were used to study cerebral amyloid angiopathy;[62] in this case, iron labeled macrophages were found in the brain, despite the fact that the blood brain barrier (BBB) was intact as verified using gadolinium magnetic resonance imaging. Circulating monocytes have been shown to migrate from the lumen into the vessel wall[63] and are able to transmigrate the BBB when attracted by chemokines produced by Aβ-stimulated cells.[64,65] Thus, the results of Beckmann et al.[62] suggest monocytes took up SPIONs from the circulation and then penetrated the brain. Further in vivo analysis of SPIONs with various surface charges should be performed to evaluate how monocyte uptake can influence the fibrillation process.

METHODS

Superparamagnetic Iron Oxide Nanoparticles (SPIONs). *Materials.* Analytical grade iron salts (iron chloride) and sodium hydroxide (NaOH) were purchased from Merck (Darmstadt, Germany) and were employed without further purification. Dextran

dx.doi.org/10.1021/cn300196n | ACS Chem. Neurosci. 2013, 4, 475−485

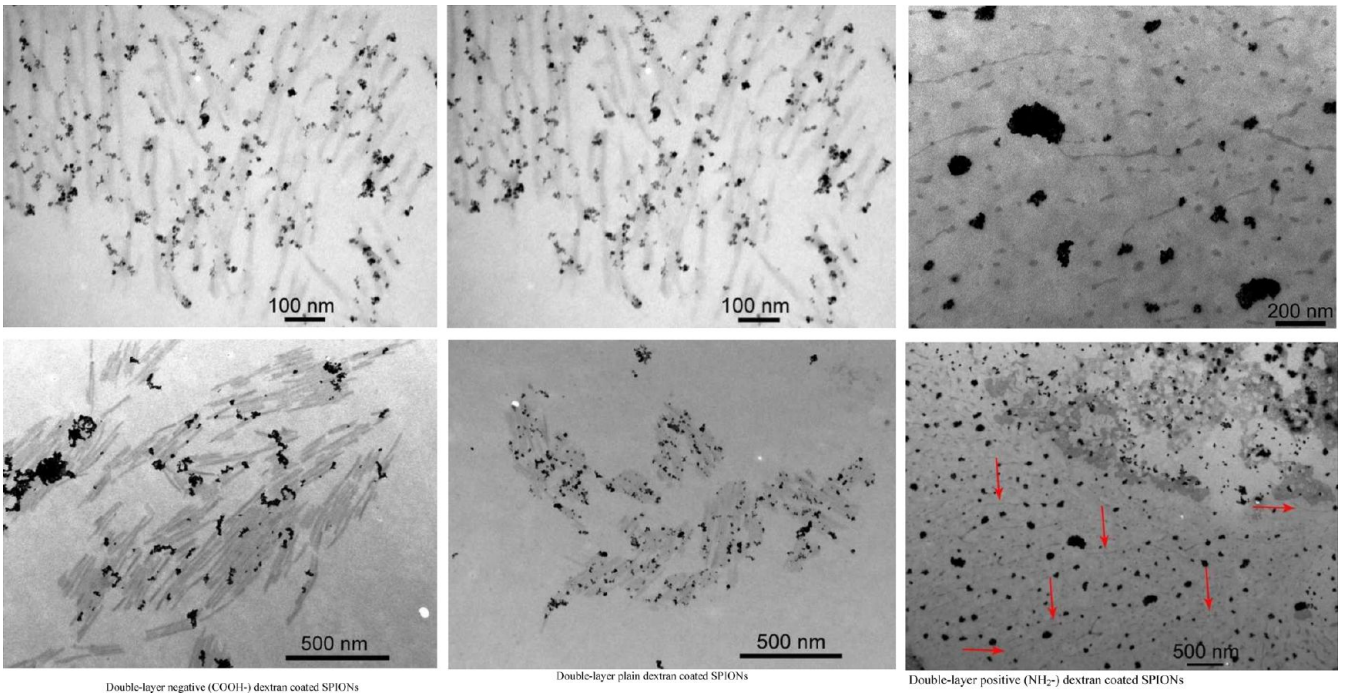

Figure 5. TEM images of Aβ fibrils after 2400 min incubation of Aβ monomers (0.5 μM) with double layer negative (left), plain (middle), and positive (right) dextran-coated SPIONs (100 μg/mL) at two different magnifications. In the case of the positively charged dextran-coated SPIONs, only very small fibrils are observed (see red arrows).

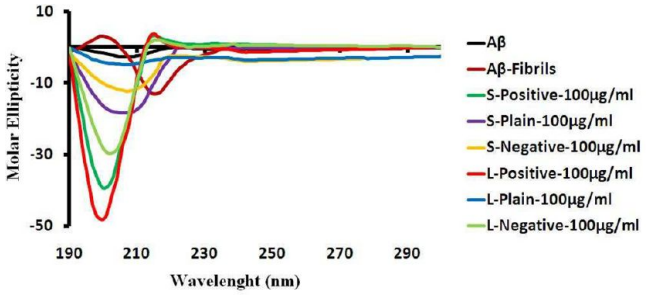

Figure 6. Circular dichroism signatures obtained for Aβ (0.5 μM), alone after 100 min and 1340 min incubation, and for mixtures of Aβ and all types of dextran-coated SPIONs (100 μg/mL) after 1340 min.

with average M_w = 5000 Da, dimethyl sulfoxide, sodium periodate, potassium cyanide, and ammonium persulfate were purchased from Sigma-Aldrich (St. Louis, MO). Carboxylated-dextran and amino-dextran were prepared according to the procedures reported by Usher and Wallis,[66,67] and Saboktakin et al.,[68] respectively.

Synthesis of the Ultrasmall SPIONs with Various Surface Characteristics. In order to ensure deoxygenation of deionized (DI) water, the DI water underwent bubbling with neutral gas (argon) for a time period of 30 min. The iron salts ($FeCl_3$ (0.086 M (3 mL)) and $FeCl_2$ (0.043 M (3 mL))) were dissolved in separate beakers containing the deoxygenated DI water. The obtained iron salt solutions were blended together, with a molar fraction adjusted to 2 (Fe^{3+}/Fe^{2+}). Dextrans (carboxylated dextran, plain dextran, and amino conjugated dextran) were dissolved in 10 mL of deoxygenated DI water. The dextran/iron mass ratio was fixed at 2.[69] The dextran solutions were mixed with the iron salt solutions (50:50 V:V (total volume of 10 mL)) and introduced into a three-neck flask equipped with a homogenizer stirring at 10 000 rpm. This procedure was done separately for the 3 types of dextran solutions in order to prepare Fe_3O_4 NPs with various surface coatings and thus zeta potentials (i.e., negative (carboxylated), neutral (plain), and positive (amine conjugated) NPs). Actual formation of NPs was triggered via dropwise addition of base medium (NaOH) to the prepared dextran-iron salt mixtures with vigorous stirring under argon protection.

In order to achieve a good size distribution, the NPs in the flask were transferred to an ultrasonic bath (100 W) which created a turbulent flow.[70] In this way, the mass transfer rate,[70] which may allow NPs to combine and build larger polycrystalline NPs was decreased. After 1 h, the black NP suspension was magnetically washed using a strong magnetic field gradient produced by a permanent Nd−Fe−B magnet and the dextran-coated Fe_3O_4 NPs were recovered. The supernatant was completely removed, and the Fe_3O_4 NPs were redispersed in DI water multiple times. As an additional step to ensure the removal of unreacted iron cations and free dextran macromolecules, the obtained ferrofluid was dialyzed using a membrane bag with a 50 kDa molecular weight cutoff (MWCO) for 24 h. The resulting purified ferrofluid was kept at 4 °C. The prepared SPIONs with their various surface chemistries are shown schematically in Figure 1, and the analysis data is given in Table 1.

Preparation of Double-Coated SPIONs with Various Surface Characteristics. The three types of dextrans were dissolved in DI water, with the same concentration as in the previous section. The various dextran-coated SPIONs synthesized in the previous section were returned to the reactor under vigorous agitation (i.e., amino-coated SPIONs were added to the amino-dextral solution for a second layer of coating, etc.). After 1 h, the double-coated SPIONs were collected by strong magnet and purified, as described above.

Amyloid Beta. Amyloid beta peptide Aβ(1−42) was synthesized by the W. M. Keck Foundation, Biotechnology Resource Laboratory (Yale University), with 80% purity (the remaining 20% of the lyophylized material is mainly water and some residual trifluoroacetic acid).

Aβ(1−42) was dissolved in a 50:50 mixture of 1% NH_4OH and 100 mM Tris buffer followed by ultracentrifugation (65 000 rpm; 1 000 000g) for 1 h at 4 °C in a Beckman ultracentrifuge in order to remove pre-existing amyloid fibrils. The upper 75% of the supernatant was carefully collected, and the concentration of Aβ(1−42) was measured using the amount of absorbance at 275 nm according to the following equation:

$$C = A/\varepsilon \quad (1)$$

dx.doi.org/10.1021/cn300196n | ACS Chem. Neurosci. 2013, 4, 475−485

where C is the concentration in moles, A is the absorption (arbitrary units), and ε is an extinction coefficient (M^{-1} cm^{-1}). In order to make solutions with desired concentrations, the supernatant was diluted to 0.05−50 μM using 13 mM sodium phosphate buffer, 0.02% NaN_3, pH 7.4. This solution was used immediately for experiments.

ThT Fluorescence Assay. A common method for evaluation (either ex vivo or in vitro) of the fibrillogenes process is the Thioflavin T (ThT) fluorescence assay. ThT is a benzothiazole dye that exhibits enhanced fluorescence (with excitation and emission at 440 and 480 nm, respectively) upon binding to amyloid fibrils and profibrils. The ThT fluorescence assays were conducted as described in several reports.[59,71] For the continuous experiments, 90 μL of the optimal concentration of Aβ(1−42) with 200 μM ThT per well was incubated in the absence or presence of various SPIONs (10 μL of the various SPIONs at concentrations from 40 to 100 μg/mL) at 37 °C and shaken at 700 rpm in NUNC 96-well black polypropylene microwell plates. The ThT fluorescence was measured through the bottom of the plate every 20 min using a Varioscan Flash plate reader from Thermo Fischer, from 20 to 1340 min (with the predetermined excitation and emission of ThT), with continuous shaking at 700 rpm and 37 °C between readings. For the control wells, 10 μL of solution without SPIONs (i.e., DI water) was added to the wells. Each experimental point is an average of the fluorescence signal from five wells containing aliquots of the same solution consisting of SPIONs and Aβ or Aβ in the absence of SPIONs.

To assess the effect of pH on Aβ fibrillation (in the absence of SPIONs), Aβ solutions with different pH (i.e., pH 2−12) were prepared by adding the acidic solution (i.e., sodium phosphate buffer) to the basic solution. The obtained kinetic data were analyzed assuming that the typical sigmoidal behavior in order to extract the kinetic parameters of the bimodal fibrillation process. An empirical sigmoidal equation was used:[72,73]

$$y = y_0 + \frac{y_{max} - y_0}{1 + e^{-(t-t_{1/2})k}} \quad (2)$$

Where y is the fluorescence intensity at time t, y_0 and y_{max} are the initial and maximum fluorescence intensities, respectively, $t_{1/2}$ is the time required to reach half the maximum intensity, and k is the apparent first-order aggregation constant. In addition, the lag time can be defined using the following equation:

$$\text{lag time} = t_{1/2} - \frac{2}{k} \quad (3)$$

The ThT fluorescence assays in the presence of SPIONs with no Aβ were used to confirm that there is no binding between the ThT dye and the SPIONs.

Circular Dichroism. In order to probe the secondary structure of Aβ after interaction with the various SPIONs, circular dichroism (CD) was employed, using an Aviv Model 202 CD spectrometer. CD spectra were recorded at room temperature; the wavelength step was 1 nm, three scans were taken per sample in the range from 190 to 300 nm, and the averaging time was 1 s at each wavelength. It is notable that the SPIONs, themselves, induce scattering in CD, as reported previously,[74] which must be considered in the interpretation of the CD data.

Transmission Electron Microscopy (TEM). A volume of 0.5 μL of dispersion (Aβ or Aβ plus SPIONs) was transferred onto carbon coated 300 mesh-Cu grids and blotted with filter paper. Fibrils were stained with 3% uranyl acetate (5 μL for 1 min), blotted, and air-dried. Transmission electron microscopy analysis was conducted on an FEI Tecnai 12 TEM (FEI Company, Eindhoven, The Netherlands) equipped with a Gatan CCD camera Model 792 (Gatan, Inc., Pleasanton, CA) at an accelerating voltage of 120 kV.

SPION Characterization. Dynamic light scattering (DLS) measurements were performed with a Malvern PCS-4700 instrument equipped with a 256-channel correlator. The 488.0 nm line of a Coherent Innova-70 Ar ion laser was used as the incident beam. The laser power used was 250 mW. The scattering angles, θ, employed ranged between 40° and 140°. The temperature was maintained at 25 °C with an external circulator. Zeta potential determination was performed using a Malvern Zetasizer 3000HSa instrument. Each measurement was an average of six repetitions of 1 min each and repeated five times. Statistical data analysis has been performed according to standard procedures, and interpreted through a cumulant expansion of the field autocorrelation function to the second order. Moreover, in order to obtain a distribution of decay rates, a constrained regularization method, CONTIN, was used to invert the experimental data.

■ ASSOCIATED CONTENT

Supporting Information

Characterization of samples and full CD results. This material is available free of charge via the Internet at http://pubs.acs.org.

■ AUTHOR INFORMATION

Corresponding Author

*(M.M.) Web: www.biospion.com. E-mail: Mahmoudi@tums.ac.ir. (I.L.) E-mail: Iseult.Lynch@cbni.ucd.ie.

Funding

M.M. was funded via an ESF EpitopeMap RNP Exchange grant to visit CBNI, which is gratefully acknowledged. Parts of this work were conducted under the framework of the INSPIRE programme, funded by the Irish Government's Programme for Research in Third Level Institutions, Cycle 4, National Development Plan 2007-2013 (M.M.). Additional funding from EU FP7 Small Collaborative project NeuroNano (NMP4- from EU FP7 Small Collaborative project NeuroNano (NMP4-SL-2008-214547, I.L.) and NanoQuébec to the Facility for Electron Microscopy Research at McGill University is also acknowledged.

Notes

The authors declare no competing financial interest.

■ REFERENCES

(1) Cleary, J. P., Walsh, D. M., Hofmeister, J. J., Shankar, G. M., Kuskowski, M. A., Selkoe, D. J., and Ashe, K. H. (2005) Natural oligomers of the amyloid-beta protein specifically disrupt cognitive function. *Nat. Neurosci. 8*, 79−84.

(2) Walsh, D. M., Klyubin, I., Shankar, G. M., Townsend, M., Fadeeva, J. V., Betts, V., Podlisny, M. B., Cleary, J. P., Ashe, K. H., Rowan, M. J., and Selkoe, D. J. (2005) The role of cell-derived oligomers of abeta in alzheimer's disease and avenues for therapeutic intervention. *Biochem. Soc. Trans. 33*, 1087−1090.

(3) Selkoe, D. J. (2002) Alzheimer s disease is a synaptic failure. *Science 298*, 789−791.

(4) Lambert, M. P., Barlow, A. K., Chromy, B. A., Edwards, C., Freed, R., Liosatos, M., Morgan, T. E., Rozovsky, I., Trommer, B., Viola, K. L., Wals, P., Zhang, C., Finch, C. E., Krafft, G. A., and Klien, W. L. (1998) Diffusible, nonfibrillar ligands derived from Ab1−42 are potent central nervous system neurotoxins. *Proc. Natl. Acad. Sci. U.S.A. 95*, 6448−6453.

(5) Walsh, D., Klyubin, I., Fadeeva, J. V., Cullen, W. K., Anwyl, R., Wolfe, M. S., Rowan, M. J., and Selkoe, D. J. (2002) Naturally secreted oligomers of amyloid b protein potently inhibit hippocampal long-term potentiation in vivo. *Nature 416*, 535−539.

(6) Lansbury, P. T. J. (1997) Inhibition of amyloid formation: A strategy to delay the onset of Alzheimer's disease. *Curr. Opin. Chem. Biol. 1*, 260−267.

(7) Walsh, D. M., and Selkoe, D. J. (2007) Abeta Oligomers a decade of discovery. *J. Neurochem. 101*, 1172−1184.

(8) Nelson, R., and Eisenberg, D. (2006) Structural models of amyloid-like fibrils. *Adv. Protein Chem. 73*, 235−282.

(9) Walsh, D. M., Hartley, D. M., Kusumoto, Y., Fezoui, Y., Margaret, M., Condron, M. M., Lomakin, A., Benedek, G. B., Selkoe, D. J., and Teplow, D. B. (1999) Amyloid betaprotein fibrillogenesis. Structure

and biological activity of protofibrillar intermediates. *J. Biol. Chem. 274*, 25945−25952.
(10) Guo, M., Gorman, P. M., Rico, M., Chakrabartty, A., and Laurents, D. V. (2005) Charge substitution shows that repulsive electrostatic interactionsimpede the oligomerization of Alzheimer amyloid peptides. *FEBS Lett. 579*, 3574−3578.
(11) Liu, R. T., McAllister, C., Lyubchenko, Y., and Sierks, M. R. (2004) Residues 17−20 and 30−35 of beta-amyloid play critical roles in aggregation. *J. Neurosci. Res. 75*, 162−171.
(12) Lowe, T. L., Strzelec, A., Kiessling, L. L., and Murphy, R. M. (2001) Structure-function relationships for inhibitors of beta-amyloid toxicity containing the recognition sequence KLVFF. *Biochemistry 40*, 7882−7889.
(13) Sidhartha, M. C., Hinke, M., Maarten, M., Meijer, E. W., David, V., Hilal, A. L., Frank, B., and Wiep, S. (2007) Branched KLVFF Tetramers strongly potentiate inhibition of beta-amyloid aggregation. *ChemBioChem 8*, 1857−1864.
(14) Bett, C. K., Ngunjiri, J. N., Serem, W. K., Fontenot, K. R., Hammer, R. P., McCarley, R. L., and Garno, J. C. (2010) Structurea Activity Relationships in Peptide Modulators of Amyloid Protein Aggregation: Variation in Disubstitution Results in Altered Aggregate Size and Morphology. *ACS Chem. Neurosci. 1*, 608−626.
(15) Norde, W. (2000) *Physical Chemistry of Biological Interfaces* (Baszkin, A., and Norde, W., Eds.), p 115, Marcel Dekker, New York.
(16) Tjernberg, L. O., Callaway, D. J. E., Tjernberg, L. O., Hahne, S., Lilliehook, C., Terenius, L., Thyberg, J., and Nordstedt, C. (1999) A molecular model of Alzheimer amyloid b-peptide fibril formation. *J. Biol. Chem. 274*, 12619−12625.
(17) Guo, M., Gorman, P. M., Rico, M., Chakrabartty, A., and Laurents, D. V. (2005) Charge substitution shows that repulsive electrostatic interactions impede the oligomerization of Alzheimer amyloid peptides. *FEBS Lett. 579*, 3574−3578.
(18) Fraser, P. E., Nguyen, J. T., Surewicz, W. K., and Kirschner, D. A. (1991) pH-dependent structural transitions of Alzheimer amyloidpeptides. *Biophys. J. 60*, 1190−1201.
(19) Laurent, S., Ejtehadi, M. R., Rezaei, M., Kehoe, P. G., and Mahmoudi, M. (2012) Interdisciplinary challenges and promising theranostic effects of nanoscience in Alzheimer's disease. *RSC Adv. 2*, 5008−5033.
(20) Fraser, P., McLachlan, D., Surewicz, W., Mizzenqq, C., Snow, A., Nguyen, J., and Kirschner, D. A. (1994) Conformation andfibrillogenesis of Alzheimer Ab peptides with selected substitution of charged residues. *J. Mol. Biol. 244*, 64−73.
(21) Necula, M., Kayed, R., Milton, S., and labe, C. G. (2007) Small molecule inhibitors of aggregation indicate that amyloid beta oligomerization and fibrillization pathways are independent and distinct. *J. Biol. Chem. 282*, 10311−10324.
(22) Kim, J. E., and Lee, M. (2003) Fullerene inhibits betaamyloid peptide aggregation. *Biochem. Biophys. Res. Commun. 303*, 576−579.
(23) Hashimoto, M., Shahdat, H. M., Katakura, M., Tanabe, Y., Gamoh, S., Miwa, K., Shimada, T., and Shido, O. (2009) Effects of docosahexaenoic acid on in vitro amyloid beta peptide 25−35 fibrillation. *Biochim. Biophys. Acta 1791*, 289−296.
(24) Sun, Y., Zhang, G., Hawkes, C. A., Shaw, J. E., McLaurin, J., and Nitz, M. (2008) Synthesis of scylloinositol derivatives and their effects on amyloid beta peptide aggregation. *Bioorg. Med. Chem. 16*, 7177−7184.
(25) Cohen, T., Frydman-Marom, A., Rechter, M., and Gazit, E. (2006) Inhibition of amyloid fibril formation and cytotoxicity by hydroxyindole derivatives. *Biochemistry 45*, 4727−4735.
(26) Linse, S., Cabaleiro-Lago, C., Xue, W. F., Lynch, I., Lindman, S., Thulin, E., Radford, S. E., and Dawson, K. A. (2007) Nucleation of protein fibrillation by nanoparticles. *Proc. Natl. Acad. Sci. U.S.A. 104*, 8691−8696.
(27) Wu, W. H., Sun, X., Yu, Y. P., Hu, J., Zhao, L., Liu, Q., Zhao, Y. F., and Li, Y. M. (2008) TiO2 nanoparticles promote beta-amyloid fibrillation in vitro. *Biochem. Biophys. Res. Commun. 373*, 315−318.
(28) Klajnert, B., Cortijo-Arellano, M., Cladera, J., and Bryszewska, M. (2006) Influence of dendrimer's structure on its activity against amyloid fibril formation. *Biochem. Biophys. Res. Commun. 345*, 21−28.
(29) Cabaleiro-Lago, C., Quinlan-Pluck, F., Lynch, I., Lindman, S., Minogue, A. M., Thulin, E., Walsh, D. M., Dawson, K. A., and Linse, S. (2008) Inhibition of amyloid beta protein fibrillation by polymeric nanoparticles. *J. Am. Chem. Soc. 130*, 15437−15443.
(30) Cabaleiro-Lago, C., Quinlan-Pluck, F., Lynch, I., Dawson, K. A., and Linse, S. (2010) Dual Effect of Amino Modified Polystyrene Nanoparticles on Amyloid β Protein Fibrillation. *ACS Chem. Neurosci. 1*, 279−287.
(31) Mahmoudi, M., Hosseinkhani, H., Hosseinkhani, M., Broutry, S., Simchi, A., Journeay, W. S., Subramani, K., and Laurent, S. (2011) Magnetic Resonance Imaging Tracking of Stem Cells in Vivo Using Iron Oxide Nanoparticles as a Tool for the Advancement of Clinical Regenerative Medicine. *Chem. Rev. 111*, 253−280.
(32) Mahmoudi, M., Milani, A. S., and Stroeve, P. (2010) Synthesis, surface architecture and biological response of superparamagnetic iron oxide nanoparticles for application in drug delivery: a review. *Int. J. Biomed. Nanosci. Nanotechnol. 1*, 164−201.
(33) Mahmoudi, M., and Shokrgozar, M. A. (2012) Multifunctional stable fluorescent magnetic nanoparticles. *Chem. Commun. 48*, 3957−3959.
(34) Mahmoudi, M., Simchi, A., and Imani, M. (2010) Recent Advances in Surface Engineering of Superparamagnetic Iron Oxide Nanoparticles for Biomedical Applications. *J. Iran. Chem. Soc. 7*, S1−S27.
(35) Nighoghossian, N., Wiart, M., Cakmak, S., Berthezène, Y., Derex, L., Cho, T.-H., Nemoz, C., Chapuis, F., Tisserand, G.-L., Pialat, J.-B., Trouillas, P., Froment, J.-C., and Hermier, M. (2007) Inflammatory Response After Ischemic Stroke. *Stroke 38*, 303−307.
(36) Saleh, A., Schroeter, M., Ringelstein, A., Hartung, H.-P., Siebler, M., Mödder, U., and Jander, S. (2007) Iron Oxide Particle-Enhanced MRI Suggests Variability of Brain Inflammation at Early Stages After Ischemic Stroke. *Stroke 38*, 2733−2737.
(37) Dousset, V., Brochet, B., Deloire, M. S. A., Lagoarde, L., Barroso, B., Caille, J.-M., and Petry, K. G. (2006) MR Imaging of Relapsing Multiple Sclerosis Patients Using Ultra-Small-Particle Iron Oxide and Compared with Gadolinium. *Am. J. Neuroradiol. 27*, 1000−1005.
(38) Tourdias, T., Roggerone, S., Filippi, M., Kanagaki, M., Rovaris, M., Miller, D. H., Petry, K. G., Brochet, B., Pruvo, J.-P., Radüe, E.-W., and Dousset, V. (2012) Assessment of Disease Activity in Multiple Sclerosis Phenotypes with Combined Gadolinium- and Superparamagnetic Iron Oxide−enhanced MR Imaging. *Radiology 264*, 225−233.
(39) Brambilla, D., Verpillot, R., Le Droumaguet, B., Nicolas, J., Taverna, M., Kóňa, J., Lettiero, B., Hashemi, S. H., De Kimpe, L., Canovi, M., Gobbi, M., Nicolas, V., Scheper, W., Moghimi, S. M., Tvaroška, I., Couvreur, P., and Andrieux, K. (2012) PEGylated Nanoparticles Bind to and Alter Amyloid-Beta Peptide Conformation: Toward Engineering of Functional Nanomedicines for Alzheimer's Disease. *ACS Nano 6*, 5897−5908.
(40) Mahmoudi, M., Sahraian, M. A., Shokrgozar, M. A., and Laurent, S. (2011) Superparamagnetic Iron Oxide Nanoparticles: Promises for Diagnosis and Treatment of Multiple Sclerosis. *ACS Chem. Neurosci. 2*, 118−140.
(41) Mahmoudi, M., Sant, S., Wang, B., Laurent, S., and Sen, T. (2011) Superparamagnetic iron oxide nanoparticles (SPIONs): Development, surface modification and applications in chemotherapy. *Adv. Drug Delivery Rev. 63*, 24−46.
(42) Mahmoudi, M., Stroeve, P., Milani, A. S., and Arbab, A. (2010) Superparamagnetic Iron Oxide Nanoparticles: Synthesis, Surface Engineering, Cytotoxicity and Biomedical Applications, Nova Science Publishers, Inc., ISBN: 978-1-61668-964-3.
(43) Skaat, H., Belfort, G., and Margel, S. (2009) Synthesis and characterization of fluorinated magnetic core−shell nanoparticles for inhibition of insulin amyloid fibril formation. *Nanotechnology 20*, 225106.

(44) Skaat, H., Sorci, M., Belfort, G., and Margel, S. (2009) Effect of maghemite nanoparticles on insulin amyloid fibril formation: selective labeling, kinetics, and fibril removal by a magnetic field. *J. Biomed. Mater. Res., Part A 91*, 342−351.
(45) Skaat, H., and Margel, S. (2009) Synthesis of fluorescent-maghemite nanoparticles as multimodal imaging agents for amyloid-β fibrils detection and removal by a magnetic field. *Biochem. Biophys. Res. Commun. 386*, 645−649.
(46) Viktor Andersson, B., Skoglund, C., Uvdal, K., and Solin, N. (2012) Preparation of amyloid-like fibrils containing magnetic iron oxide nanoparticles: Effect of protein aggregation on proton relaxivity. *Biochem. Biophys. Res. Commun. 419*, 682−686.
(47) Andrea, B., Eva, B., Martina, K., Peter, K., Francesco, V., Natalia, T., Milan, T., Jaroslava, B., Fabio, B., and Zuzana, G. (2010) Effect of Fe_3O_4 magnetic nanoparticles on lysozyme amyloid aggregation. *Nanotechnology 21*, 065103.
(48) Mahmoudi, M., Hofmann, H., Rothen-Rutishauser, B., and Petri-Fink, A. (2012) Assessing the in vitro and in vivo toxicity of superparamagnetic iron oxide nanoparticles. *Chem. Rev. 112*, 2323−2338.
(49) Rauch, J., Kolch, W., and Mahmoudi, M. (2012) Cell Type-Specific Activation of AKT and ERK Signaling Pathways by Small Negatively-Charged Magnetic Nanoparticles. *Sci. Rep. 2*, 868.
(50) Mahmoudi, M., and Serpooshan, V. (2012) Silver-Coated Engineered Magnetic Nanoparticles Are Promising for the Success in the Fight against Antibacterial Resistance Threat. *ACS Nano. 6*, 2656−2664.
(51) Ikeda, K., Okada, T., Sawada, S.-i., Akiyoshi, K., and Matsuzaki, K. (2006) Inhibition of the formation of amyloid β-protein fibrils using biocompatible nanogels as artificial chaperones. *FEBS Lett. 580*, 6587−6595.
(52) Olmedo, I., Araya, E., Sanz, F., Medina, E., Arbiol, J., Toledo, P., Álvarez-Lueje, A., Giralt, E., and Kogan, M. J. (2008) How Changes in the Sequence of the Peptide CLPFFD-NH2 Can Modify the Conjugation and Stability of Gold Nanoparticles and Their Affinity for β-Amyloid Fibrils. *Bioconjugate Chem. 19*, 1154−1163.
(53) Kirschner, D. A., Inouye, H., Duffy, L. K., Sinclair, A., Lind, M., and Selkoe, D. J. (1987) Synthetic peptide homologous to protein from Alzheimer disease forms amyloid-like fibrils in vitro. *Proc. Natl. Acad. Sci. U.S.A. 84*, 6953−6957.
(54) Tjernberg, L. O., Naslund, J., Lindqvist, F., Johansson, J., Karlstrom, A. R., Thyberg, J., Terenius, L., and Nordstedt, C. (1996) Arrest of beta-amyloid fibril formation by a pentapeptide ligand. *J. Biol. Chem. 271*, 8545−8548.
(55) Gordon, D. J., Sciarretta, K. L., and Meredith, S. C. (2001) Inhibition of β-amyloid(40) fibrillogenesis and disassembly of β-amyloid(40) fibrils by short β-amyloid congeners containing N-methyl amino acids at alternate residues. *Biochemistry 40*, 8237−8245.
(56) Gordon, D. J., Tappe, R., and Meredith, S. C. (2002) Design and characterization of a membrane permeable N-methyl amino acid-containing peptide that inhibits A. beta.1−40 fibrillogenesis. *J. Pept. Res. 60*, 37−55.
(57) Gordon, D. J., and Meredith, S. C. (2003) Probing the role of backbone hydrogen bonding in β-amyloid fibrils with inhibitor peptides containing ester bonds at alternate positions. *Biochemistry 42*, 475−485.
(58) Bieschke, J., Siegel, S. J., Fu, Y. W., and Kelly, J. W. (2008) Alzheimer's Aβ peptides containing an isostructural backbone mutation afford distinct aggregate morphologies but analogous cytotoxicity. Evidence for a common lowabundance toxic structure(s). *Biochemistry 47*, 50−59.
(59) Cabaleiro-Lago, C., Quinlan-Pluck, F., Lynch, I., Dawson, K. A., and Linse, S. (2010) Dual Effect of Amino Modified Polystyrene Nanoparticles on Amyloid β Protein Fibrillation. *ACS Chem. Neurosci. 1*, 279−287.
(60) Etienne, M. A., Aucoin, J. P., Fu, Y. W., McCarley, R. L., and Hammer, R. P. (2006) Stoichiometric inhibition of amyloid beta-protein aggregation with peptides containing alternating R,R-disubstituted amino acids. *J. Am. Chem. Soc. 126*, 3522−3523.
(61) Amiri, H., Wan, S., Mahmoudi, M., Lascialfari, A., Lynch, I., and Monopoli, M. P. (2012) Protein Corona Affects Relaxivity and MRI Contrast Efficiency of Magnetic Nanoparticles. *J. Nanopart. Res.*,.
(62) Beckmann, N., Gérard, C., Abramowski, D., Cannet, C., and Staufenbiel, M. (2011) Noninvasive Magnetic Resonance Imaging Detection of Cerebral Amyloid Angiopathy-Related Microvascular Alterations Using Superparamagnetic Iron Oxide Particles in APP Transgenic Mouse Models of Alzheimer's Disease: Application to Passive Aβ Immunotherapy. *J. Neurosci. 31*, 1023−1031.
(63) Vinters, H. V., Natté, R., Maat-Schieman, M. L. C., van Duinen, S. G., Hegeman-Kleinn, I., Welling-Graafland, C., Haan, J., and Roos, R. A. C. (1998) Secondary microvascular degeneration in amyloid angiopathy of patients with hereditary cerebral hemorrhage with amyloidosis, Dutch type (HCHWA-D). *Acta Neuropathol. 95*, 235−244.
(64) El Khoury, J., Toft, M., Hickman, S. E., Means, T. K., Terada, K., Geula, C., and Luster, A. D. (2007) Ccr2 deficiency impairs microglial accumulation and accelerates progression of Alzheimer-like disease. *Nat. Med. 13*, 432−438.
(65) Hickman, S. E., and Khoury, J. E. (2010) Mechanisms of Mononuclear Phagocyte Recruitment in Alzheimers Disease. *NS Neurol. Disord.: Drug Targets 9*, 168−173.
(66) Usher, T. C., and Wallis, S. H. (2004) Process of Making Carboxilated Dextran, U.S. Patent US6 703 499.
(67) Martwiset, S., Koh, A. E., and Chen, W. (2006) Nonfouling Characteristics of Dextran-Containing Surfaces. *Langmuir 22*, 8192−8196.
(68) Saboktakin, M. R., Tabatabaie, R. M., Maharramov, A., and Ramazanov, M. A. (2010) A synthetic macromolecule as MRI detectable drug carriers:Aminodextran-coated iron oxide nanoparticles. *Carbohydr. Polym. 80*, 695−698.
(69) Mahmoudi, M., Simchi, A., Milani, A. S., and Stroeve, P. (2009) Cell toxicity of superparamagnetic iron oxide nanoparticles. *J. Colloid Interface Sci. 336*, 510−518.
(70) Mahmoudi, M., Simchi, A., Imani, M., Milani, A. S., and Stroeve, P. (2008) Optimal design and characterization of superparamagnetic iron oxide nanoparticles coated with polyvinyl alcohol for targeted delivery and imaging. *J. Phys. Chem. B 112*, 14470−14481.
(71) Betts, V., Leissring, M. A., Dolios, G., Wang, R., Selkoe, D. J., and Walsh, D. M. (2008) Aggregation and catabolism of disease-associated intra-A beta mutations: Reduced proteolysis of A beta A21G by neprilysin. *Neurobiol. Dis. 31*, 442−450.
(72) Nielsen, L., Khurana, R., Coats, A., Frokjaer, S., Brange, J., Vyas, S., Uversky, V. N., and Fink, A. L. (2001) Effect of environmental factors on the kinetics of insulin fibril formation: Elucidation of the molecular mechanism. *Biochemistry 40*, 6036−6046.
(73) Kodaka, M. (2004) Requirements for generating sigmoidal time-course aggregation in nucleation-dependent polymerization model. *Biophys. Chem. 107*, 243−253.
(74) Mahmoudi, M., Sardari, S., Shokrgozar, M. A., Laurent, S., and Stroeve, P. (2011) Irreversible changes in protein conformation due to interaction with superparamagnetic iron oxide nanoparticles. *Nanoscale 3*, 1127−1138.